Growth cones as soft and weak force generators

Timo Betz[a,b,1], Daniel Koch[a], Yun-Bi Lu[a,c], Kristian Franze[a,c], and Josef A. Käs[a]

[a]Division of Soft Matter Physics, Department of Physics, Universität Leipzig, Linnéstrasse 5, 04103 Leipzig, Germany; [b]Laboratoire Physico-chimie Curie (Unité mixte de recherche 168), 11, rue Pierre et Marie Curie, 75231 Paris Cedex 05, France; and [c]Paul-Flechsig-Institute for Brain Research, Department of Neurophysiology, University of Leipzig, Jahnallee 59, 04109 Leipzig, Germany

Edited by Thomas D. Pollard, Yale University, New Haven, CT, and approved June 30, 2011 (received for review May 12, 2011)

Many biochemical processes in the growth cone finally target its biomechanical properties, such as stiffness and force generation, and thus permit and control growth cone movement. Despite the immense progress in our understanding of biochemical processes regulating neuronal growth, growth cone biomechanics remains poorly understood. Here, we combine different experimental approaches to measure the structural and mechanical properties of a growth cone and to simultaneously determine its actin dynamics and traction force generation. Using fundamental physical relations, we exploited these measurements to determine the internal forces generated by the actin cytoskeleton in the lamellipodium. We found that, at timescales longer than the viscoelastic relaxation time of $\tau = 8.5 \pm 0.5$ sec, growth cones show liquid-like characteristics, whereas at shorter time scales they behaved elastically with a surprisingly low elastic modulus of $E = 106 \pm 21$ Pa. Considering the growth cone's mechanical properties and retrograde actin flow, we determined the internal stress to be on the order of 30 pN per μm^2. Traction force measurements confirmed these values. Hence, our results indicate that growth cones are particularly soft and weak structures that may be very sensitive to the mechanical properties of their environment.

motility | neuron | elasticity | mechanics | scanning force microscopy

Neuronal growth is a fundamental event during ontogenetic development and nerve regeneration. The mechanical forces required for neuronal pathfinding and translocation are generated in the growth cone, a motile extension at the neurite tip (1). As in other motile structures, growth cone movement involves actin polymerization and myosin motor mediated contraction of the actin network in the lamellipodium, a flat structure internally made up by a cross-linked actin network (2). The movement of the leading edge is determined by the difference between outward pushing actin polymerization and the continuous centripetal flow of actin, called the retrograde flow (3) (Fig. S1). Local measurements of the retrograde flow (3, 4) and traction forces of filopodia (5, 6) have been reported on various substrate stiffness. These observations and the detailed analysis of neuron branching on substrates of varying stiffness (7) highlight the importance of the mechanical environment for neuronal growth. Furthermore, the constant neurite tension that is maintained by molecular motors in the neurite cytoskeleton has been extensively studied (8–10). However, neither the internal forces, which are the forces generated and acting within the growth cone, nor the growth cone's lamellipodial traction forces have yet been quantified. To understand the mechanics of neuronal growth, knowledge of the relation between the growth cone's viscoelastic material properties, the internally generated forces and the traction forces transmitted to the substrate is of fundamental importance.

A recent study used speckle microscopy and a simple spring model to convert data from retrograde flow in epithelial cells into qualitative internal stresses (11). Whereas this model allowed a qualitative derivation of the internal stress, it only modeled the elastic contribution, thus neglecting the viscous dissipation that is dominant at longer timescales. Furthermore, as the material properties of the cell were not determined, this approach did not allow a quantitative force calculation. On the other hand, theoretical work has been published that uses mean field theory models to describe the viscous regime of lamellipodial actin flows by expanding liquid crystal physics to active systems (12). Here we extend these purely elastic (11) and viscous (12) analyses by considering the inherent viscoelastic nature of a cell from a mechanical point of view.

The main scope of this study is to provide a measurement of the internal and external stress generated by the actin cytoskeleton of a moving growth cone. It should be noted that stress and force give similar information, because stress is defined by a force per area. As all the following measurements are based on image analysis, the fundamental property measured is stress. We first establish the characteristic mean viscoelastic material properties of a growth cone and then combine these with the material flow fields as determined by speckle microscopy to determine the stress required for the observed flow. Finally, we exploit traction force microscopy to obtain a complete picture of the intra- and extracellular stresses that eventually result in neuronal growth cone motility.

Deducing Forces From Deformation

Common experience tells us that objects can be deformed upon application of a force. In the example of a simple spring, there is a linear relation between force and deformation, summarized in Hooke's law for an elastic spring: $F = k \times x$, where F is the force that is required to deform a spring with spring constant k by a distance x. Hence, knowing the spring constant and the deformation, it is straight forward to deduce the force responsible for the observed deformation. Another well known deformation is the flow of a liquid, where the viscous forces are independent of the actual deformation magnitude, but depend on the deformation rate or flow velocity. Living cells, however, are neither ideally elastic nor ideally fluid objects, but show both characteristics simultaneously. This needs to be taken into account for any quantitative description. Typically, living cells show viscous characteristics at long time scales, whereas they are rather elastic at short times. These viscoelastic material properties are described by the time dependent viscoelastic relaxation modulus E(t). In the case of a three dimensional cell, in general, the viscoelastic modulus is a fourth-order tensor. However, this complexity can be drastically reduced by applying the approximation that the elastic properties are in first order homogeneous and isotropic. These two general assumptions allow to describe a viscoelastic material by two fundamental properties, namely the time dependent relaxation modulus E(t) and the Poisson's ratio ν. We directly measure these two material properties of a growth cone using a modified scanning force microscopy (SFM) technique (13, 14) Once the material properties are known, it is straight forward to determine the relation between deformation u_{ij} and stress tensor σ_{ij}

Author contributions: T.B. and J.A.K. designed research; T.B., D.K., Y.-B.L., and K.F. performed research; K.F. contributed new reagents/analytic tools; T.B., D.K., and Y.-B.L. analyzed data; and T.B. and J.A.K. wrote the paper.

The authors declare no conflict of interest.

This article is a PNAS Direct Submission.

[1]To whom correspondence should be addressed. E-mail: timo.betz@curie.fr.

This article contains supporting information online at www.pnas.org/lookup/suppl/doi:10.1073/pnas.1106145108/-/DCSupplemental.

(σ = Force/Area) that reads (see *Appendix* and *SI Text* for a detailed derivation):

$$\sigma_{ij}(t) = \int_{-\infty}^{t} \frac{E(t-\tau)}{1+\nu}\left(\frac{du_{ij}}{d\tau} + \frac{\nu}{1-2\nu}\frac{du_{kk}}{d\tau}\delta_{ij}\right)d\tau. \qquad [1]$$

This equation describes how the stress at a given time depends on the material properties (E(t) and ν) and the deformation velocity (du/dt). The integral over the time passed ensures that the history of the deformation is taken into account. This history dependence presents the difference between a purely elastic versus a viscoelastic deformation because a viscoelastic material such as a cell has a memory effect represented by the time dependence of E(t).

Results and Discussion

Viscoelastic Properties of the Growth Cone. We determined the viscoelastic material properties of neuronal growth cones using SFM-based microrheology (13, 14), which measures the frequency dependent elastic storage modulus $E'(f)$ and viscous loss modulus $E''(f)$. We measured $E'(f)$ and $E''(f)$ for five different frequencies in the range of 0.3–30 Hz (Fig. 1). To extract the time dependent relaxation modulus E(t), we fitted $E'(f)$ and $E''(f)$ to an extended Kelvin–Voigt model (Fig. 1, *SI Text*, and Fig. S2), which has been previously shown to approximate cellular deformations in the measured frequency range (15). Whereas the fit quality shows that this model provides an adequate approximation, it is also evident that a complete description requires more refined models, which are out of scope of the presented work. Furthermore, it should be noted that the technique used cannot well resolve small spatial variations of the mechanical properties as the size of the probe limits the spatial resolution to approximately 2 μm. Thus the measured values directly represent average viscoelastic properties for the whole growth cone. The good reproducibility of the data with an average relative error of 21% ($n = 64$, 11 growth cones) in the 10 measurement points (two points for five frequencies) shows that the applied measurement indeed gives a reasonable approximation of the material properties. Hence, the small error justifies the approximation of spatial and temporal homogeneity as applied in the mathematical description.

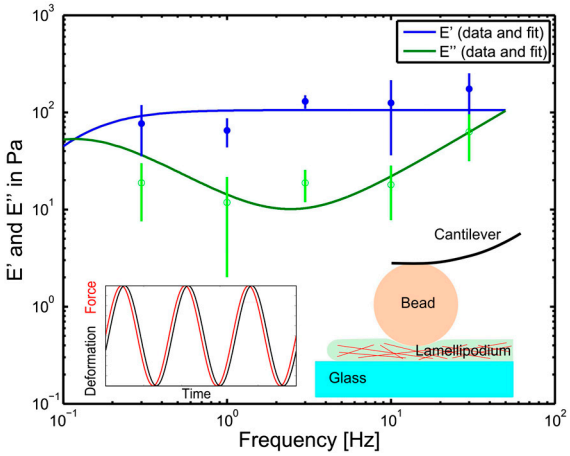

Fig. 1. Rheological measurements of the frequency dependent Young's modulus of growth cones. Filled circles represent the storage modulus, whereas open circles give the loss modulus. The lines represent the fit according to the extended Voigt model as described in *SI Text*. It should be noted that for the low frequency measurements (below 1 Hz) the data is less reliable as the active retrograde flow can not be neglected in the long time regime, whereas the fit model does not consider such activity. At low frequencies the loss modulus becomes more important than the storage modulus, thus marking a viscous regime, whereas at higher frequencies, the growth cone behaves more like an elastic object. According to the model, it is possible to identify a plateau for the storage modulus, which gives a steady state Young's modulus of $E = 106 \pm 21$ Pa. The sketch and the inset illustrate the measurement method. A bead, glued to the cantilever of a SFM, penetrates the lamellipodium with an oscillating force (*Inset*, red), whereas the resulting deformation (*Inset*, black) is measured. The amplitude and the phase difference between force and deformation determine the viscoelastic properties at the oscillation frequency.

The fit of $E'(f)$ and $E''(f)$ presented in Fig. 1 depends on three independent fit parameters for the growth cone: the Young's modulus $E = 106 \pm 21$ Pa, the steady state viscosity $\eta = 905 \pm 26$ Pa s and the relaxation time $\tau_R = 8.5 \pm 0.5$ s. The Poisson ratio $\nu = 0.47 \pm 0.05$ (mean ± SEM; $n = 64$) was directly determined from the SFM measurements, as previously described (13, 14). It should be stressed that the Young's modulus E and the relaxation modulus $E(t)$ are different quantities. Whereas the Young's modulus E is a constant that describes the purely elastic stiffness of the material represented by the plateau (Fig. 1), the relaxation modulus $E(t)$ is a function that includes the time dependence of the viscous deformation of the growth cone. Our data is consistent with previously published values for central nervous system (CNS) cells (14) and CNS tissue (16, 17). Interestingly, the measured elastic plateau at $E = 106 \pm 21$ Pa is surprisingly soft as compared to other motile cell types such as fibroblasts or fish keratocytes, which typically show elastic moduli in the range of kilopascal (18, 19). The measured Young's modulus presents a natural limit for the load (i.e., maximal stresses) that can be transmitted to the underlying substrate. Such a maximal load may be imposed by the tension within the distal neurite that has to be balanced by the growth cone. Based on the measured Young's modulus, we estimated a maximal neurite tension of 8 nN (Young's modulus times area: $F_{max} \approx E \times r_{gc}^2 \times \pi \approx 8$ nN) that a typical growth cone can sustain (radius: $r_{gc} \approx 5$ μm). This upper limit is consistent with measurements, as it is well above previously reported maximum neurite tensions of about 2 nN (20, 21). The measured Young's modulus further indicates that the maximal traction forces generated in a growth cone should be significantly smaller than those found in stiffer cell types such as fibroblasts or fish keratocytes (22, 23).

Internal Stress of the Actin Cytoskeleton. To quantify the internal stress $\vec{\sigma}(x,y)$ within the growth cone, the viscoelastic material properties, and the deformation rate of the actin cytoskeleton (i.e., the retrograde flow fields $\vec{u}(x,y)$; see Fig. S1) need to be determined. It should be noted that the calculation assumes that the 2D retrograde flow detection captures all the information, and that flows in the out of plain direction are not relevant in the lamellipodium. The calculation can be separated into four steps (further explained in *SI Text*). First, the retrograde flow is calculated. Subsequently, the stress required to explain the deformation between subsequent images is calculated. In a third step, the deformation history is included in the calculation. This step makes use of the fact that stress from the previous deformation has not yet been fully dissipated. Finally, the forces are calculated based on the local gradient of the stress tensor. In more detail, the steps are:

1. *Quantification of retrograde flow.* To extract the lamellipodial actin dynamics, we used a feature tracking algorithm inspired by speckle microscopy (24, 25). Fluorescence microscopy time-series of growth cones from GFP-actin transfected NG108-15 cells were recorded with a time resolution of 3–5 s (see Movie S1). In contrast to most previous measurements of neuronal retrograde flow (3, 26), our technique measures the flow fields of filamentous actin (F-actin) within the whole growth cone (25) (Fig. S1 and Movie S2). We find a mean retrograde flow velocity for NG108-15 growth cones of 1.46 ± 0.60 μm/min (mean ± SEM; $n = 19$). The measured retro-

grade flow shows a centripetal alignment and a strong decrease of retrograde flow toward the transition zone between the actin filled lamellipodium and the microtubule dominated central region. This confirms the well described properties of retrograde flow as reported in the literature (3, 26), and raises the question of the origin, distribution and dynamics of the forces that drive the observed flow.

2. *Calculation of the stress field between successive images.* This step does only consider the deformation between two successive images. We assume that the flow is constant during a time interval, which simplifies the integral of Eq. **1** (details in *Appendix* and *SI Text*). Hence, this step does only extract the stress that is required to explain the deformation between two successive images, and it does not yet take into account the accumulation of stress due to the history of the system.
3. *Accumulation of stress and relaxation by the deformation history.* To obtain the full stress at a given moment, we add up all the stresses of the previous deformations to the current stress calculated in step 2. Stress relaxes over time following an exponential decay with time constant $\tau_R = 8.5 \pm 0.5$ s that leads to a relaxation below 1% after 40 s. To include the entire stress history, we sum all the partially relaxed stresses from previous deformations. When the stress measured at previous time points is dissipated to less than 1% of its initial value, we do not further consider it. This strategy includes both, the actual measured deformation, and the stress history according to the viscoelastic material properties. It should be noted that the transport of stress according to the measured deformation is also taken into account. This is important, because local stresses are created in the actin network of the lamellipodium, and are thus transported with the retrograde flow.
4. *Final calculation of the internal forces.* Here, we use the stress tensor field calculated in the previous step to gain the internal force field. This is done by applying the local equilibrium condition Eq. **6**, where we calculate the local gradient of the stress tensor, which has to be balanced by an internal stress. This is equivalent to Newton's laws. This calculation yields the internal force for each pixel, so it is again in units of stress.

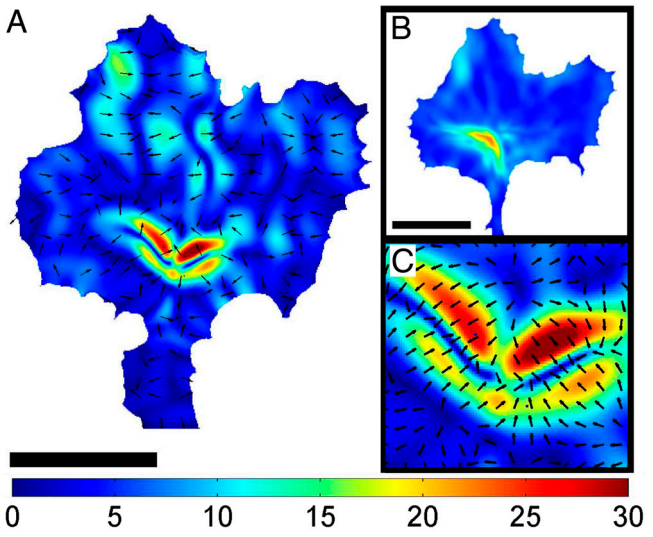

Fig. 2. Internal stress within a neuronal growth cone. (*A*) Distribution of the momentary internal stress field in a neuronal growth cone. The color coding gives the stress magnitude in units of force per area (Pa = pN/μm^2), and the black arrows indicate the stress direction. Scale bar is 10 μm. (*B*) Time averaged mean stress distribution of a full time series of internal stress fields ($t = 10$ min). The stress is highest in the transition zone, and decays toward the edge. (*C*) A close-up on the central part of the stress field in (*A*) shows that the internal stresses are contractile and arranged like dipoles.

Resulting internal stresses are presented in Fig. 2 (Movie S3). The internal stress distribution shows localized foci within the transition zone at which they converge, resulting in a mean peak stress of $\langle \sigma^{\mathrm{Int}}_{\mathrm{Peak}} \rangle = 40.1 \pm 17$ Pa (median ± STD; $n = 119$; with one Pa = 1 pN/μm^2). These spots were highly dynamic and generally appeared and disappeared within 30–60 s. Hence, the peak stresses are an order of magnitude higher than the overall average stress that is found by averaging over the full area of a growth cone: $\langle \sigma^{\mathrm{Int}} \rangle = 5.8 \pm 0.3$ Pa (mean ± STD; $n = 119$). To study the spatial distribution of stress, we average over a 10 min time period. This is done by calculating the average over the recording time for each pixel. The resulting distribution of stress magnitudes is presented in Fig. 2*B*. This analysis reveals that on average the stresses are mainly produced at the transition zone and decay toward the edge. The measured internal stresses at the transition zone are contractile, as demonstrated by the opposing stress directions in the enlarged area shown in Fig. 2*C*. This is consistent with the forces dipoles generated by Myosin II (27) pulling on two neighboring actin filaments with opposing force directions. In addition our analysis provides a full quantification of the internal force amplitude and direction as well as the stress tensors with a spatial resolution that is only limited by the resolution of the underlying retrograde flow detection. Therefore, we provide a powerful analytic tool to determine forces by simply analyzing the retrograde flow fields.

Traction Stress of Neuronal Growth Cones. To further validate the obtained values of the internal stress calculation we used traction force microscopy (TFM) (22, 28) to independently measure the stresses that are finally transmitted to the substrate by the growth cone. As the traction forces originate from the internal forces, the magnitude of the traction stress should be consistent with the magnitude of the internal stress and therefore provide an independent control measurement to the presented calculation. TFM measures the stress of a growth cone adhered to an elastic polyacrylamide (PAA) gel substrate by detecting the movement of fluorescent beads embedded at the surface of the gel. The Young's modulus of the PAA gel was determined to be $E_{\mathrm{PAA}} = 200 \pm 20$ Pa using an SFM. To measure integrin mediated traction forces, we coated the PAA gel with laminin. Similar to the calculation of the intracellular forces, once the elastic parameters of the substrate and its deformation as caused by the growth cones are known, the traction forces can be determined (22, 28). We find that the traction forces act close to the edge of the growth cone (Fig. 3*A*), where most substrate attachments are found (29). The average peak traction stress of 26.7 ± 2.6 Pa is in excellent agreement with the determined internal forces. This further supports our finding that growth cones are mechanically soft and weak force generators compared to other cell types such as fibroblasts [traction force: approximately 1 kPa (30)] or migrating epithelial cells [traction force: approximately 200 Pa (31)], both having elastic moduli in the kilopascal range (18, 19). The low stresses that we observed for neuronal growth cones are consistent with our findings of low elastic strength and low internal forces. Our results indicate that there may be a direct correlation between cell rigidity, internal forces, and traction forces coupled to the substrate. We can further speculate about a possible relation between cell rigidity and the preference for certain substrate rigidity. Stiff cells such as fibroblasts have been found to prefer stiff substrates (32) whereas neurons prefer soft substrates that are comparable to the elasticity of glial cells (7, 14). However, it should be noted that there are also soft cells such a astrocytes that prefer growing on stiff substrates (33). Further investigation will be required to understand to which extend there may be a fundamental relation or if these similarities are purely random.

The total stress acting in a growth cone is a combination of the internal stress and the traction stress. Because the growth cone exerts traction forces on the substrate, local force balance

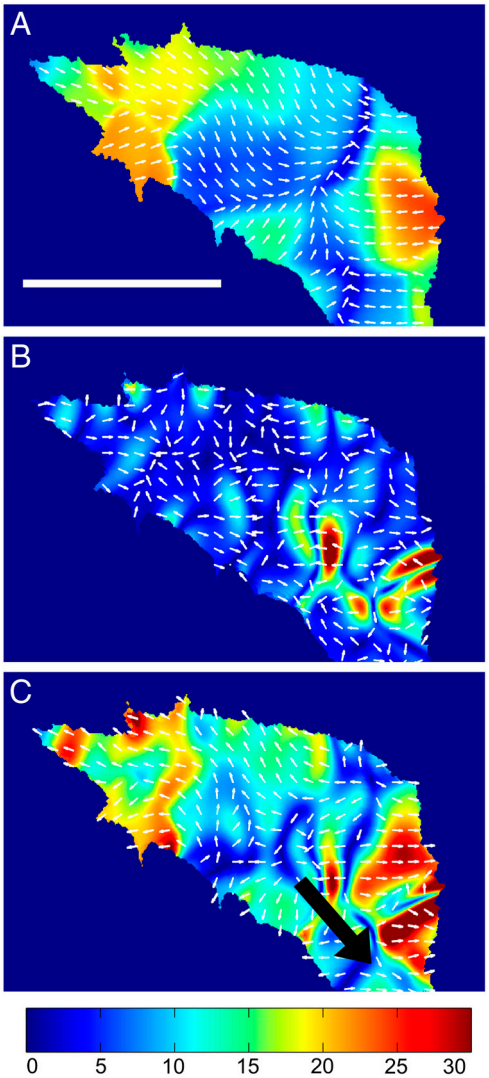

Fig. 3. Traction stress, internal stress, and the combined total stress of a neuronal growth cone. (*A*) Traction stress distribution of a neuronal growth cone. (*B*) Internal stress field of growth cone shown in *A*. Contractile stresses are localized at the central domain of the growth cone. (*C*) The total stress field of the growth cone reveals that the forces are generated at the central domain, and the cross-linked actin network transmits the stress to the substrate adhesions in the peripheral region. The black arrow represents the pulling force with which the neurite is pulling on the growth cone. (*A*–*C*) Color code gives stress magnitude in Pa. Scale bar is 10 μm.

requires that the growth cone feels exactly the opposite forces from the substrate. As we are interested in the stress acting on the actin network in the lamellipodium, the traction stress felt by the growth cone is the opposite stress as measured using TFM. Consequentially, to gain the full stress fields of a growth cone, the traction stress vectors have to be subtracted from the internal stress vectors to yield the total stress acting inside: $\sigma^{\text{Total}}(\vec{x}) = \sigma^{\text{Internal}}(\vec{x}) - \sigma^{\text{Traction}}(\vec{x})$. The total stress field arising from our model for the stress generation mechanism is shown in Fig. 3*C* (see also Movies S4 and S5). The measured traction forces can also be used to directly determine the neurite pulling force, or neurite tension. As a matter of fact, the sum of the traction stress over the growth cone area does not fully match up, as it should for a stationary object. The reason for this mismatch is that we need to consider the neurite pulling force, which is equivalent to the neurite tension (5, 34). Consequently, the sum up of the traction stress is a measure of the neurite tension. We find a net force or neurite tension of $F_{\text{Net}} = 602 \pm 149$ pN, which is in good agreement with previously reported values (20, 35).

Summary of the Determined Viscoelastic Forces on the Actin Cytoskeleton. To summarize our findings we propose a simple scheme as shown in Fig. 4. Contractile stresses are generated at the force foci in the transition zone (Fig. 2*A* and Fig. 3*C*). The viscoelastic actin network in the lamellipodium partially transmits these forces to the leading edge where the forces are coupled to the substrate via adhesion sites, whereas part of the energy is dissipated by the viscoelastic deformation of the actin network and the substrate clutch. The contractile forces do furthermore compensate for the neurite tension that is constantly pulling on the growth cone. This neurite tension has been extensively studied in the literature (10) and it is well known that it originates from the contraction of the neurite cytoskeleton (8–10).

The force transmission toward the substrate depends partially on the interaction between the actin network and the substrate, which is mediated by actin to integrin force transmission, but also by the mechanical properties of the lamellipodium. This clutch mechanism of force transmission has been well documented in the literature (6, 36–38), but the underlying molecular details are yet to be understood. As we show in this work, the actin network in the lamellipodium is a viscoelastic material, and hence the force transmission strongly depends on its viscoelastic properties, a fact that should be considered when investigating the force clutch mechanism, as not only the actin to integrin connection, but also the actin network itself presents a viscous flow. In the long time regime (>10 s) the viscous effects dominate, and therefore any force transmission requires flow. In this view it becomes clear that the actin network in the lamellipodium has to deform steadily to maintain a constant force transmission to the substrate. From a mechanical point of view our results may also explain why even in stationary growth cones a steady and fast retrograde flow is observed. Without the continuous polymerization and viscous flow, the actin network could not sustain the continuous neurite tension and would simply disintegrate and loose its substrate adhesions. This in turn would lead to a retraction of the

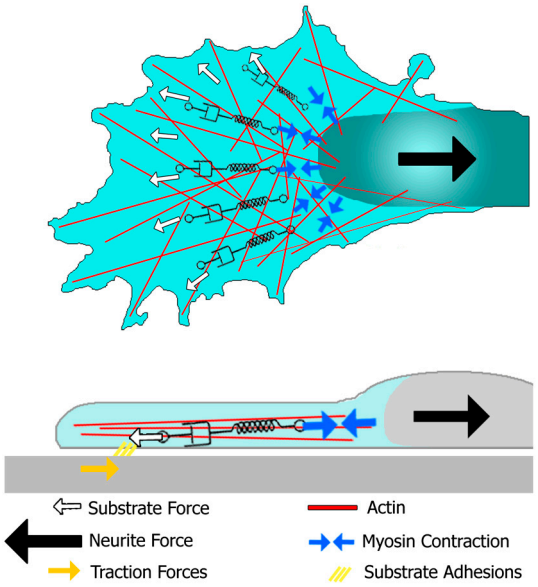

Fig. 4. Summarizing scheme of the forces involved in the actin cytoskeleton in growth cone motility. External forces such as neurite tension (black arrow) and the substrate stress (white arrows) are transmitted to the contracting myosin motors (blue arrows) by the viscoelastic actin networks of the lamellipodium and the actin cortex of the neurite. In this model, the effective link between these two types of forces are the force generating myosin motors in the transition zone.

whole growth cone, as the pulling forces of the neurite need to be balanced by transmitting them to the substrate, which requires sufficiently strong lamellipodial rigidity and substrate adhesion. Hence, the steady flow allows even soft viscoelastic structures like the growth cone to bear the constant tension generated in the neurite.

Conclusion

Neuronal growth is a highly specialized type of cell motility that appears to be mechanically optimized for the movement in soft environments. The neuronal growth cones' weak forces and low elastic stiffness may indicate an important adaptation to the soft tissue found in the brain: glial cells provide a soft mechanical substrate with rather small elastic moduli of E approximately 300 Pa (14). The passive and active mechanical properties of neuronal growth cones investigated in this study provide a plausible mechanical framework for the preference of neurons for soft substrates (7). In addition, our results may explain why it is necessary to keep the energy consuming retrograde flow running even when the growth cone is in a resting phase and does not move extensively. Our results suggest that the continuous retrograde flow allows maintaining the substrate traction forces that are required to prevent growth cone retraction by the neurite tension. If the flow would cease, the viscoelastic characteristics of the lamellipodium would result in a simple relaxation of any transmitted stresses within a few seconds, leading to an immediate retraction of the whole structure due to neurite tension. Regarding biomechanics and force generation, the presented work allows the speculation that there may be a fundamental relation between the mechanical properties of a growth cone and the mechanical properties of the environment. Growth cone mechanics could therefore optimize navigation in soft environments, and mechanics could even be an additional guidance cue on top of all the biochemical guidance cues already identified to control neuronal growth. Further investigation on the role of mechanics in neuronal navigation will yield unique insights into the complex behavior of neuronal navigation.

Materials and Methods

Preparation of Elastic Polyacrylamide Substrates. A modified version of the protocol published by Wang and Pelham (28) was used. Briefly, as bottom plate round coverslips (diameter: 20 mm; VWR) were cleaned and then covered with 400 μL of 0.1N NaOH, which was evaporated using a hotplate. Subsequently, coverslips were covered with 200 μL of 3-aminopropyltrimethoxy silane (Sigma) for 5 min, rinsed with Millipore water and treated with 0.5% glutaraldehyde for 30 min to finalize the coating. As nonadherent surface, microscope slides were pretreated to prevent any adhesion to PAA. After cleaning, a thin film of SurfaSil (Perbio Science) was applied to the slides using either a cotton swab or a small cotton cloth. Subsequently, the film was cleaned off using a cotton swab or cloth and the slides were submerged in methanol to finalize the reactions. The composition of PAA determines the elastic properties of the final gel, and for the presented experiments, 170 μL of 40% acrylamide solution (Sigma) and 30 μL of 2% bis-acylamid (Sigma) were added to 1,750 μL PBS, yielding a final concentration of 3.5% acrylamide and 0.03% bis-acrylamide. Fluorescent beads were embedded into the gel by addition of 20 μL bead solution (Fluo Sphere, 100 nm diameter, 2%, Molecular Probes). Polymerization was started by adding 8 μL of 10% (w/v) ammonium persulfate (Sigma) and catalyzed by 12 μL of N,N,N′,N′-tetramethylethylenediamine (Sigma). A drop of 14 μL solution was added onto the inert microscope slides and the silanized coverslips were put onto the drop, with the treated side down. The polymerization finished within 30 min. Using scanning force microcopy (SFM), the elasticity of the gel was measured to be $E_{PAA} = 200 \pm 20$ Pa.

For surface modification, 1.5 μg Sulfo-SANPAH (Perbio Science) was dissolved in 20 μL DMSO, and then 1980 μL of a 20 mM Hepes solution with a pH of 8.5 was added to the solution. One hundred microliters of the final solution were added to each of the PAA gels, which were subsequently stored in the dark for 30 min and then photoactivated for 5 min using a strong UV lamp (Model B, Blak-Ray). The activated solution was carefully washed off using 20 mM Hepes solution. After washing three times with PBS, 100 μL poly-L-lysine (Sigma) was added to each gel and stored at 4 °C over night. Finally, gels were washed three times in PBS, and 100 μL of a 40 μg/mL laminin (Sigma) solution were applied to the gels. Gels with laminin were incubated at 37 °C for 1 h, washed with PBS, then stored at least 24 h in cell culture medium for equilibration before cells were plated.

Cell Culture and Image Acquisition. Details are given in *SI Text*.

Microrheology. The methods used to determine the viscoelastic properties of neuronal growth cones have been described in detail before (13, 14). Briefly, we used a 5.6 μm diameter bead that was glued on the SFM cantilever and applied a sinusoidal force on the lamellipodium with a given frequency (Fig. 1, *Inset*). The applied forces and the resulting deformation were measured and the in and out of phase components were acquired using a lock-in amplifier (13). The final viscoelastic modulus for each frequency was determined by fitting the data to a viscoelastic model that takes into account the thickness of the lamellipodium, as previously discussed in the literature (13, 18).

Traction Force Microscopy. After recording the time series of GFP-actin transfected growth cones and fluorescent tracer particles embedded in the PAA gel, growth cones were removed using a combination of 0.5% trypsine and 0.5% Tween 20 (Sigma), and a reference image of the relaxed PAA gel was recorded. The deformation between the time-series images and the reference image was calculated using a cross correlation algorithm implemented in LabView (National Instruments) and Matlab (MathWorks). Finally, traction stresses were calculated following the unconstrained deconvolution method as presented in (22). The analysis method was successfully verified by reproducing an applied lateral force of 1 nN using SFM.

Appendix

To gain the forces that drive retrograde actin flow, we extended linear elasticity theory (39) to the viscoelastic regime. Viscoelasticity connects the stress σ and the strain u using the characteristic memory function, or relaxation modulus E(t) that contains information about both viscous and elastic material characteristics. If the stress resulting from a known deformation is sought, the Boltzmann superposition principle is useful (40):

$$\sigma(t) = \int_{-\infty}^{t} E(t-\tau)\frac{du}{d\tau}d\tau, \qquad [2]$$

where $\dot{u} = du/dt$ is the strain rate. If the time dependent relaxation modulus E(t) and u(t) are known, the time dependent stress can be calculated. In 3D, it is necessary to change to a tensorial description. The linear strain tensor u_{ij} is calculated at each point in the object from the deformation vector $\vec{u}$ by

$$u_{ij} = \frac{1}{2}\left(\frac{\partial u_i}{\partial x_j} + \frac{\partial u_j}{\partial x_i}\right). \qquad [3]$$

The pure elastic material properties can be described by the Young's modulus E and the Poisson ratio ν to calculate the stress by

$$\sigma_{ij} = \frac{E}{1+\nu}\left(u_{ij} + \frac{\nu}{1-2\nu}u_{kk}\delta_{ij}\right). \qquad [4]$$

Recalling the Boltzmann superposition principle (Eq. **2**), the time dependent stress can be calculated by

$$\sigma_{ij}(t) = \int_{-\infty}^{t} \frac{E(t-\tau)}{1+\nu}\left(\frac{du_{ij}}{d\tau} + \frac{\nu}{1-2\nu}\frac{du_{kk}}{d\tau}\delta_{ij}\right)d\tau. \qquad [5]$$

In a final step we calculate the internal force vectors using the local equilibrium condition that requires that any spatial stress gradient has to be balanced by an internal force:

$$f_i^{\text{int}} = -\frac{\partial \sigma_{ik}}{\partial x_k}. \qquad [6]$$

ACKNOWLEDGMENTS. We thank Jacques Prost, Klaus Kroy, Ulrich Schwarz, and Iva Tolic-Norrelykke for helpful discussions. This work was supported

by the Deutsche Forschungsgemeinschaft-Graduiertenkolleg Interneuro, Specific Targeted Research Project of the European Union, called Active Biomics, the Alexander von Humboldt Foundation [Feodor Lynen Return Fellowship (K.F.)], and Ms. Marianne Duda.

1. Chilton JK (2006) Molecular mechanisms of axon guidance. *Dev Biol* 292:13–24.
2. Franze K, Guck J (2010) The biophysics of neuronal growth. *Rep Prog Phys* 73:094601–094619.
3. Lin CH, Espreafico EM, Mooseker MS, Forscher P (1996) Myosin drives retrograde F-actin flow in neuronal growth cones. *Neuron* 16:769–782.
4. Mallavarapu A, Mitchison T (1999) Regulated actin cytoskeleton assembly at filopodium tips controls their extension and retraction. *J Cell Biol* 146:1097–1106.
5. Heidemann SR, Lamoureux P, Buxbaum RE (1990) Growth cone behavior and production of traction force. *J Cell Biol* 111:1949–1957.
6. Chan CE, Odde DJ (2008) Traction dynamics of filopodia on compliant substrates. *Science* 322:1687–1691.
7. Flanagan LA, Ju YE, Marg B, Osterfield M, Janmey PA (2002) Neurite branching on deformable substrates. *Neuroreport* 13:2411–2415.
8. Joshi HC, Chu D, Buxbaum RE, Heidemann SR (1985) Tension and compression in the cytoskeleton of PC 12 neurites. *J Cell Biol* 101:697–705.
9. Ahmad FJ, et al. (2000) Motor proteins regulate force interactions between microtubules and microfilaments in the axon. *Nat Cell Biol* 2:276–280.
10. Baas PW, Ahmad FJ (2001) Force generation by cytoskeletal motor proteins as a regulator of axonal elongation and retraction. *Trends Cell Biol* 11:244–249.
11. Ji L, Lim J, Danuser G (2008) Fluctuations of intracellular forces during cell protrusion. *Nat Cell Biol* 10:1393–1400.
12. Juelicher F, Kruse K, Prost J, Joanny JF (2007) Active behavior of the Cytoskeleton. *Phys Rep* 449:3–28.
13. Mahaffy RE, Park S, Gerde E, Kas J, Shih CK (2004) Quantitative analysis of the viscoelastic properties of thin regions of fibroblasts using atomic force microscopy. *Biophys J* 86:1777–1793.
14. Lu YB, et al. (2006) Viscoelastic properties of individual glial cells and neurons in the CNS. *Proc Natl Acad Sci USA* 103:17759–17764.
15. Wottawah F, et al. (2005) Optical rheology of biological cells. *Phys Rev Lett* 94:098103.
16. Miller K, Chinzei K, Orssengo G, Bednarz P (2000) Mechanical properties of brain tissue in vivo: Experiment and computer simulation. *J Biomech* 33:1369–1376.
17. Christ AF, et al. (2010) Mechanical difference between white and gray matter in the rat cerebellum measured by scanning force microscopy. *J Biomech* 43:2986–2992.
18. Mahaffy RE, Park S, Gerde E, Kas J, Shih CK (2004) Quantitative analysis of the viscoelastic properties of thin regions of fibroblasts using atomic force microscopy. *Biophys J* 86:1777–1793.
19. Brunner CA, et al. (2006) Cell migration through small gaps. *Eur Biophys J* 35:713–719.
20. Dennerll TJ, Joshi HC, Steel VL, Buxbaum RE, Heidemann SR (1988) Tension and compression in the cytoskeleton of PC-12 neurites. II: Quantitative measurements. *J Cell Biol* 107:665–674.
21. Bernal R, Pullarkat PA, Melo F (2007) Mechanical properties of axons. *Phys Rev Lett* 99:018301.
22. Butler JP, Tolic-Norrelykke IM, Fabry B, Fredberg JJ (2002) Traction fields, moments, and strain energy that cells exert on their surroundings. *Am J Physiol Cell Physiol* 282:C595–605.
23. Lee J, Jacobson K (1997) The composition and dynamics of cell-substratum adhesions in locomoting fish keratocytes. *J Cell Sci* 110((Pt 22)):2833–2844.
24. Danuser G, Waterman-Storer CM (2006) Quantitative fluorescent speckle microscopy of cytoskeleton dynamics. *Annu Rev Biophys Biomol Struct* 35:361–387.
25. Betz T, Koch D, Lim D, Kas JA (2009) Stochastic actin polymerization and steady retrograde flow determine growth cone advancement. *Biophys J* 96:5130–5138.
26. Medeiros NA, Burnette DT, Forscher P (2006) Myosin II functions in actin-bundle turnover in neuronal growth cones. *Nat Cell Biol* 8:216–226.
27. Bridgman PC, Dave S, Asnes CF, Tullio AN, Adelstein RS (2001) Myosin IIB is required for growth cone motility. *J Neurosci* 21:6159–6169.
28. Wang YL, Pelham RJ (1998) Preparation of a flexible, porous polyacrylamide substrate for mechanical studies of cultured cells. *Methods Enzymol* 298:489–496.
29. Gatlin JC, Estrada-Bernal A, Sanford SD, Pfenninger KH (2006) Myristoylated, alanine-rich C-kinase substrate phosphorylation regulates growth cone adhesion and pathfinding. *Mol Biol Cell* 17:5115–5130.
30. Dembo M, Wang YL (1999) Stresses at the cell-to-substrate interface during locomotion of fibroblasts. *Biophys J* 76:2307–2316.
31. Gardel ML, et al. (2008) Traction stress in focal adhesions correlates biphasically with actin retrograde flow speed. *J Cell Biol* 183:999–1005.
32. Lo C-M, Wang H-B, Dembo M, Wang Y-li (2000) Cell movement is guided by the rigidity of the substrate. *Biophys J* 79:144–152.
33. Georges PC, Miller WJ, Meaney DF, Sawyer ES, Janmey PA (2006) Matrices with compliance comparable to that of brain tissue select neuronal over glial growth in mixed cortical cultures. *Biophys J* 90:3012–3018.
34. Bray D (1979) Mechanical tension produced by nerve cells in tissue culture. *J Cell Sci* 37:391–410.
35. Bernal R, Melo F, Pullarkat PA (2010) Drag force as a tool to test the active mechanical response of PC12 neurites. *Biophys J* 98:515–523.
36. Mitchison T, Kirschner M (1988) Cytoskeletal dynamics and nerve growth. *Neuron* 1:761–772.
37. Suter DM, Forscher P (2000) Substrate—cytoskeletal coupling as a mechanism for the regulation of growth cone motility and guidance. *J Neurobiol* 44:97–113.
38. Moore SW, Biais N, Sheetz MP (2009) Traction on immobilized netrin-1 is sufficient to reorient axons. *Science* 325:166.
39. Landau LD, Lifschitz EM (1986) *Theory of Elasticity* (Pergamon, Oxford).
40. Lakes RS (1998) *Viscoelastic Solids* (CRC, Boca Raton).